Ozone and Aerosol Column Abundances Measured by the NOMAD-UVIS Spectrometer

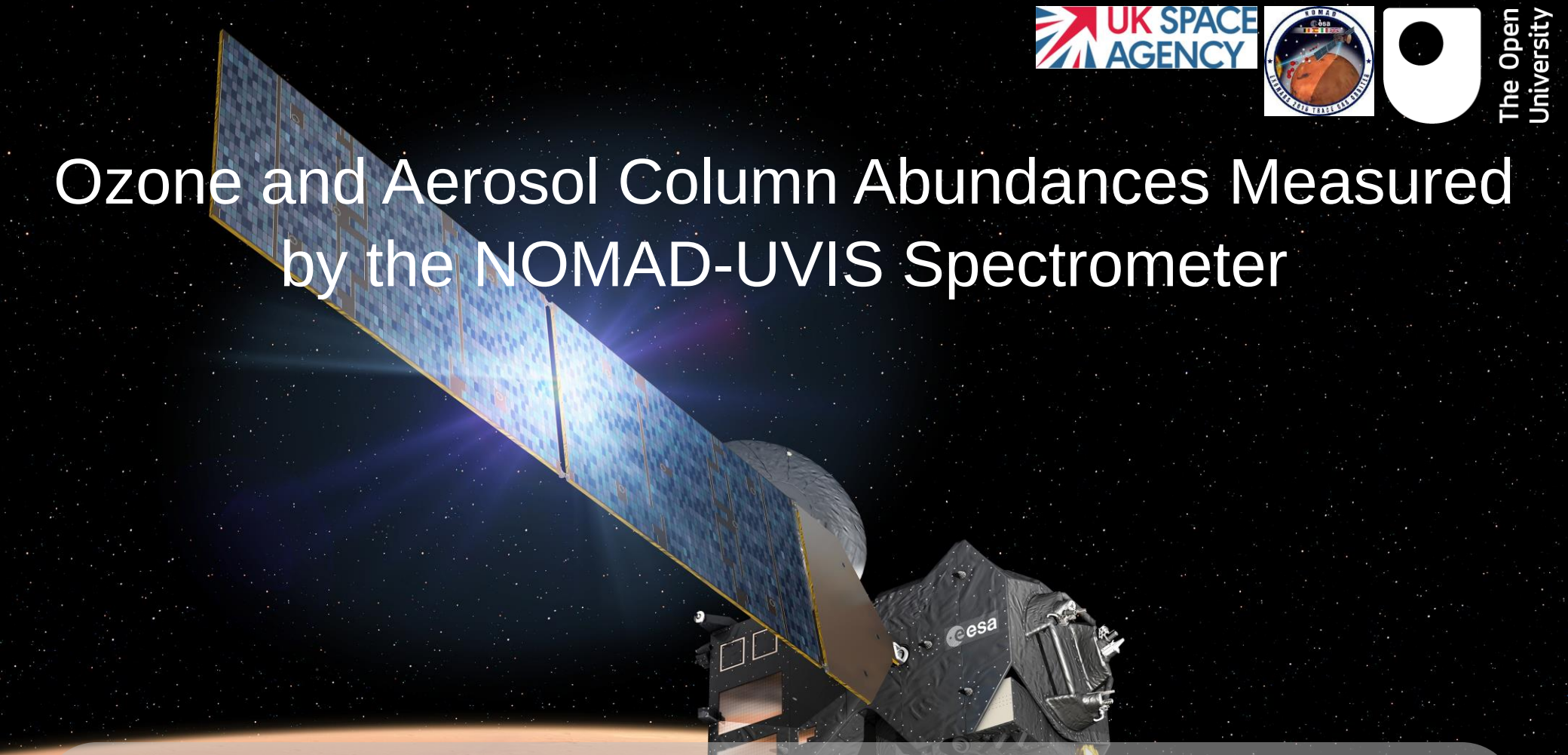

J.P. Mason[1], M.R. Patel[1,2], J.A. Holmes[1], P. Streeter[1], M. Brown[1], G. Sellers[1], C. Marriner[1], S. Lewis[1], M Wolff[3], Y. Willame[4], C. Depiesse[4], I. Thomas[4], F. Daerden[4], J.-J. Lopez-Moreno[5], G. Bellucci[6]. A.C. Vandaele[4]

[1]School of Physical Sciences, The Open University, Walton Hall, Milton Keynes MK7 6AA, U.K. (jon.mason@open.ac.uk), [2]Space Science and Technology Department, Science and Technology Facilities Council, Rutherford Appleton Laboratory, Harwell Campus, Didcot, Oxfordshire OX11 0QX, U.K, [3]Space Science Institute, Boulder, CO, U.S.A. [4]Royal Belgian Institute for Space Aeronomy, BIRA-IASB, 3 Avenue Circulaire, 1180 Brussels, Belgium. [5]Instituto de Astrofisica de Andalucía/CSIC, Granada, Spain. [6]Istituto di Astrofisica e Planetologia Spaziali, INAF, Rome, Italy.

UVIS

The Ultraviolet and Visible spectrometer (UVIS) [1] (see Fig. 1) operates in the wavelength range 200-650 nm and is the ultraviolet and visible channel of the Nadir and Occultation for MArs Discovery (NOMAD) instrument[2] onboard the ExoMars Trace Gas Orbiter (TGO). UVIS has performed high spatial, and temporal resolved, nadir observations of the Martian surface for over 3 years.

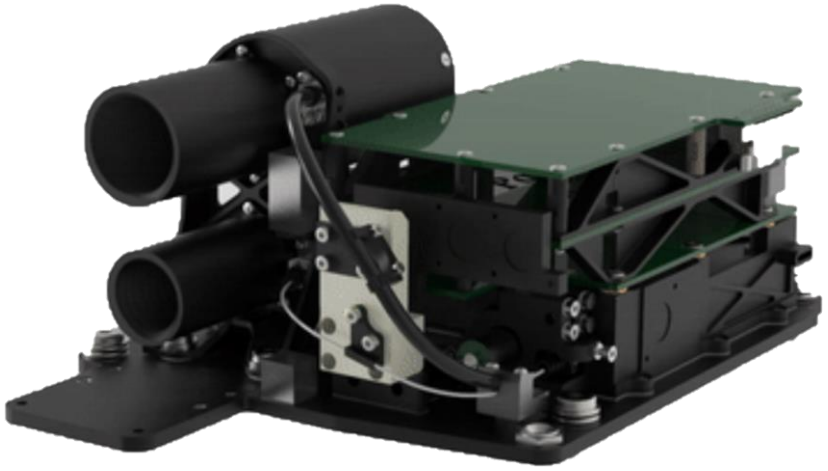

Fig 1: The UVIS spectrometer

Radiative transfer

We have used the discrete ordinates DISORT package[3] and the 'front-end' routines DISORT_MULTI[4,5,6] to develop a retrieval procedure to obtain the ozone and aerosol column abundances in the Martian atmosphere. An example of our model fit to a UVIS spectrum with strong ozone absorption is shown in Fig. 2. We fit to six wavelengths; 225, 230, 300, and 305 nm for the aerosol component, and 250 and 260 nm for ozone.

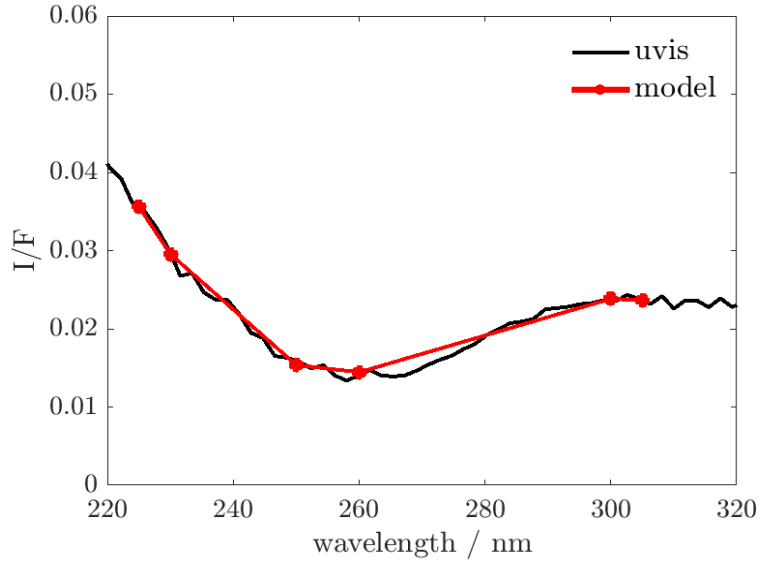

Fig 2: An example of the model fit for a UVIS nadir spectrum with strong ozone absorption.

Seasonal distribution of ozone, dust, and ice

Seasonally, the ozone distribution is consistent with low ozone abundances in equatorial regions, and higher ozone abundances at higher latitudes in the winter season. As the Martian atmosphere cools through northern spring, from the reduced solar insolation, we observe a steady increase in equatorial ozone with abundances peaking around the northern summer solstice.

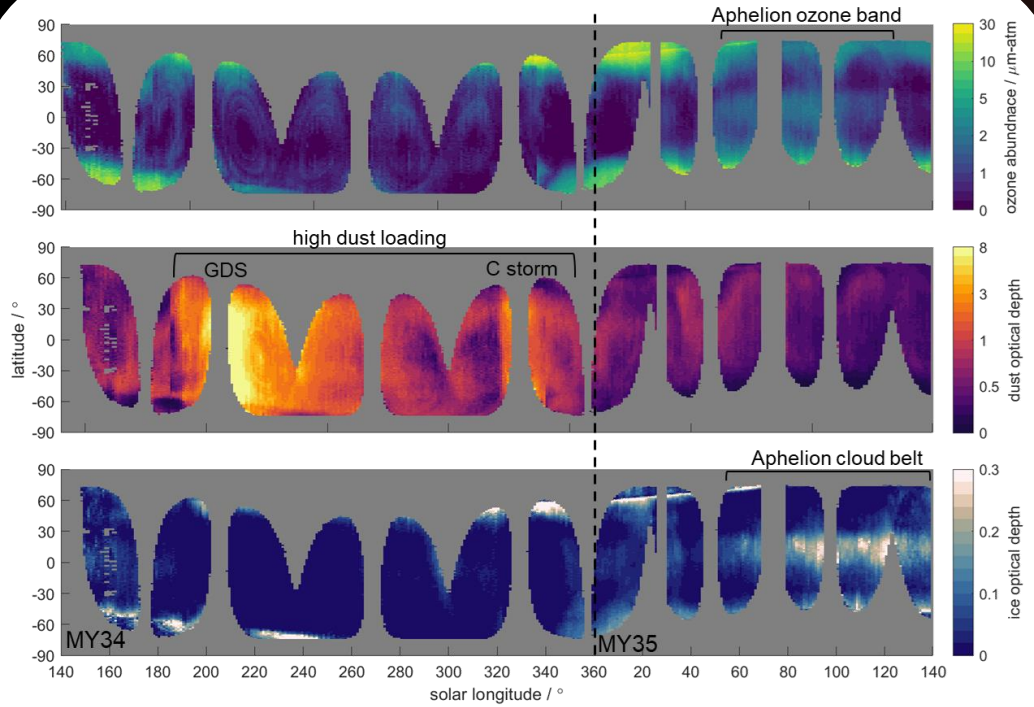

Fig 3: The seasonal distribution of ozone, dust, and ice for MY34 and the first half of MY35

Mars Year (MY) 34 was a non-typical year, experiencing a global dust storm (GDS) that started around L_s ~185º with retrieved dust column optical depths exceeding 6. The dust loading remained enhanced through southern summer, before settling back towards optical depths between 1 and 2. A second storm, the C storm, was observed at L_s ~330º where dust opacities again exceeded 2. Shortly after the C storm the dust settled back to seasonal average values of between 0.5 and 1 as the atmosphere cooled.

Water ice aerosols are observed at all latitudes prior to the onset of the GDS. As the dust loading increases, and the atmosphere warms, the ice content decreases. The initial formation of the aphelion cloud belt is observed at the end of MY34 around Ls ~340º, peaking at Ls ~90º in MY35, before decaying as the atmosphere warms.

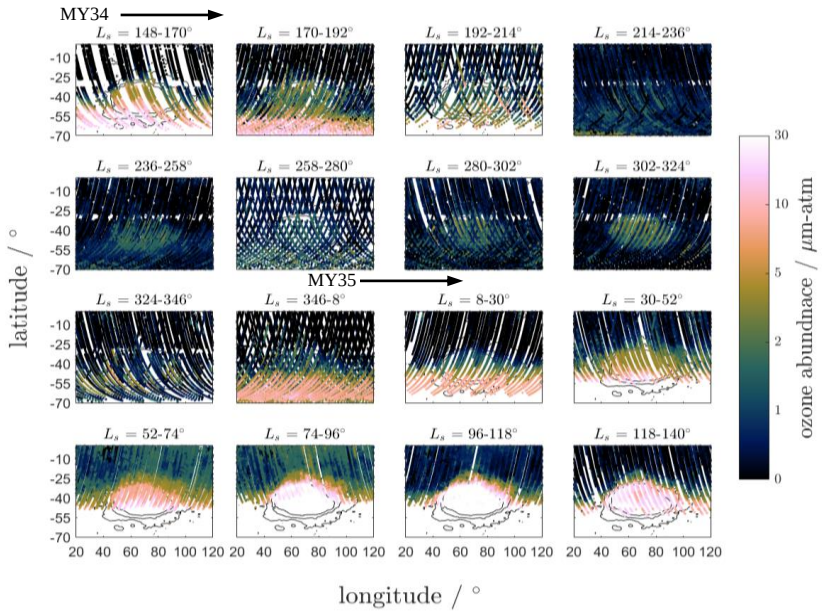

Fig 4: Ozone abundances are enhanced in Hellas basin

Ozone entrapment

The UVIS observations (Fig. 4) have shown an enhancement of ozone in large impact basins, such as Hellas Basin[6]. The entrapment of ozone within Hellas is persistent throughout MY34 and MY35 with ozone abundances of 10-20 μm-atm measured within Hellas, compared to 2-5 μm-atm outside the crater. During the GDS of MY34 ozone abundances are supressed, but still elevated at 2-5 μm-atm within the Hellas Basin.

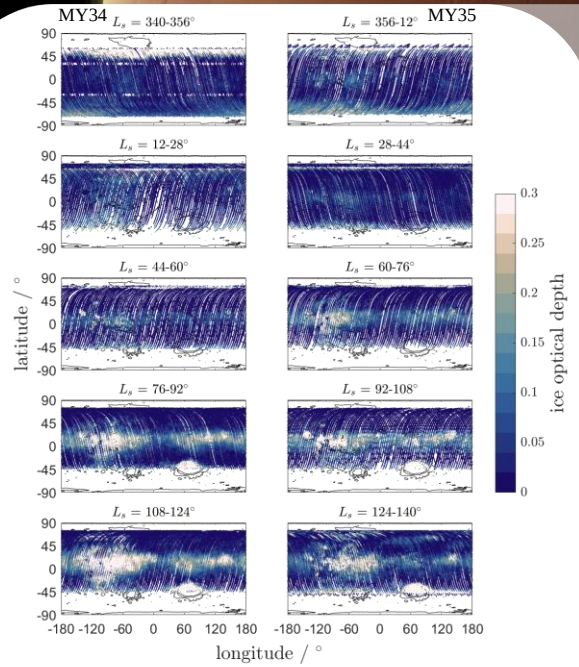

Fig 4: Formation of the aphelion cloud belt in MY35

Aphelion cloud belt

Geographically, the cloud coverage extends over all latitudes and longitudes (see Fig .5) However, there is a clear peak in ice optical depths over the Tharsis and Elysium regions. Like ozone, water-ice is enhanced over the Hellas Basin from L_s ~76º (MY35).

Further work

The TGO orbit enables measurement of ozone at different local times at the same geographical location. The ozone diurnal cycle is the focus of our current analysis.

References

[1] Patel, M R. *et al.*, *Applied* (2017). [2] Neefs, E. *et al., Applied optics* (2015). [3] Stamnes, K. *et al., Applied optics* (1988). [4] Wolff, M J. *et al., Icarus* (2010). [5] Wolff, M J. *et al., Icarus* (2019). [6] Clancy, R. T. *et al., Icarus* (2016).

Acknowledgements

The NOMAD experiment is led by the Royal Belgian Institute for Space Aeronomy (IASB-BIRA), with Co-PI teams in the United Kingdom (Open University), Spain (IAA-CSIC) and Italy (INAF-IAPS). This work was enabled through UK Space Agency grants ST/V002295/1, ST/V005332/1, ST/S00145X/1 and ST/R003025/1, and this project acknowledges funding by the Belgian Science Policy Office (BELSPO), with the financial and contractual coordination by the ESA Prodex Office (PEA 4000103401, 4000121493), by Spanish Ministry of Science and Innovation (MCIU) and by European funds under grants PGC2018-101836-B-I00 and ESP2017-87143-R (MINECO/FEDER), as well as by the Italian Space Agency through grant 2018-2-HH.0. This work was supported by the Belgian Fonds de la Recherche Scientifique – FNRS under grant number 30442502 (ET_HOME). The IAA/CSIC team acknowledges financial support from the State Agency for Research of the Spanish MCIU through the 'Center of Excellence Severo Ochoa' award for the Instituto de Astrofísica de Andalucía (SEV-2017-0709). US investigators were supported by the National Aeronautics and Space Administration.